Laser Vibrometer Measurement of Guided Wave Modes in Rail Track

Philip W. Loveday and Craig S. Long

Sensor Science and Technology, CSIR Material Science and Manufacturing,

Box 395, Pretoria 0001, South Africa. Email: ploveday@csir.co.za

ABSTRACT

The ability to measure the individual modes of propagation is very beneficial during the development of guided wave ultrasound based rail monitoring systems. Scanning laser vibrometers can measure the displacement at a number of measurement points on the surface of the rail track. A technique for estimating the amplitude of the individual modes of propagation from these measurements is presented and applied to laboratory and field measurements. The method uses modal data from a semi-analytical finite element model of the rail and has been applied at frequencies where more than twenty propagating modes exist. It was possible to measure individual modes of propagation at a distance of 400m from an ultrasonic transducer excited at 30 kHz on operational rail track and to identify the modes that are capable of propagating large distances.

KEYWORDS: Semi-analytical finite element method; modes of guided wave propagation; laser vibrometer measurement; rail track

PACs NUMBERS: 43.40.Cw; 43.20.Mv

1. INTRODUCTION

Guided wave ultrasound is well suited to the inspection or monitoring of one – dimensional waveguides such as rail track as a length of rail may be inspected from a

single transducer location. Various options for exploiting guided waves in rail applications have been investigated and were reviewed in [1]. In general, the use of guided wave ultrasound for NDE of rails requires knowledge of the characteristics of the modes of propagation; how these modes interact with the defects that are to be detected and approaches to exploit transducer arrays to selectively transmit and receive selected modes and control their direction of propagation.

Inspection or monitoring systems generally operate at frequencies where a number of modes of propagation exist. Analysis of the modes of propagation, in waveguides with complex cross – section and at high frequencies, requires numerical techniques. The semi-analytical finite element (SAFE) method is highly efficient for this purpose and has been implemented by a number of research groups [2]–[8]. The SAFE method can also be combined with conventional three – dimensional finite elements to create a hybrid model that can be used to determine the interaction between guided wave modes and defects in the rail [9] [10]. In such methods the defect is modelled in a finite element volume, with SAFE regions to either side to represent the semi – infinite incoming and outgoing waveguides with arbitrary cross - sections. Incident wave mode amplitudes are specified and the reflected and transmitted wave modes are computed. The method presented in [10] has been applied to investigate defects in rails [11]. Development of transducers or transducer arrays to effectively excite or sense specific modes of propagation may also be based on SAFE models of the rail. Three – dimensional finite elements were used to model piezoelectric transducers attached to a waveguide represented by SAFE [12], [13] and have been used to design powerful transducers.

Modelling tools are therefore well developed but the models require experimental verification. In addition, there are some parameters that have to be measured such as the attenuation of guided wave modes with distance in real rail track where the boundary conditions are complex. The development of transducers also requires measurement of the modes propagated by the transducer to ensure that the selected modes are effectively excited. During production of transducers mode propagation measurements can also be used as a measure of the performance of a transducer, which is required to ensure repeatability.

The availability of scanning laser vibrometers offers the opportunity to accurately measure the displacement (or velocity) at a large number of measurement points in a relatively short time. From these time signals an approach to estimate the modes of propagation as well as the amplitude and phase of each mode is required. This paper proposes a method for achieving this.

The more general problem of measuring the wave propagation characteristics of waveguides has been attempted in different ways by various researchers. Alleyne and Cawley [14] applied a two-dimensional Fourier transform analysis to extract the amplitude and velocity of Lamb waves. The output of the method was a three-dimensional surface plot of the frequency - wavenumber dispersion curves where the height of the surface indicated the amplitude of the wave. The method required a number of equally spaced measurement points to achieve wavenumber resolution, with 64 measurement points used in the results presented. The low frequency waves, a_0, a_1, s_0 and s_1 were extracted. Thompson [15] performed measurements of low frequency wave propagation in a rail using an array of 9 accelerometers placed at one

cross – section of the rail and an impact hammer excitation at 21 locations along the rail axis applied in the vertical and lateral directions. The measurements were performed very close to the excitation so decaying traveling waves would be encountered. A time-domain curve-fitting procedure was used to extract the amplitude and wavenumber of a number of exponential functions. The method extracted some of the known waves, up to a frequency of 6 kHz, but also produced a number of 'fictitious' waves. Lanza di Scalea and McNamara [16] applied time-frequency analysis, based on the Gabor wavelet transform, to extract the low frequency modes of propagation in a rail. The method requires only a single excitation and one or two detection points. The method was applied to a rail excited with an impact hammer and sensed with an accelerometer. The group velocity of some modes was estimated and appeared to be qualitatively, if not quantitatively, correct.

Hayashi and Murase [17] extracted the modes propagating in a pipe by measuring the time response at eight different circumferential positions at the same axial distance from the source. The extraction technique exploited the orthogonality of the modes in the circumferential direction. The modes were extracted by summing the signals from the transducers with weighting factors appropriate for that mode. This provides a time signal for each extracted mode. In the case of a cylinder the circumferential displacement distributions of the modes are known and are independent of frequency. The axial wavenumber changes with frequency but as the transducers are all at the same axial location this does not need to be accounted for. It was proposed that the same approach could be applied to extract time signals for a particular mode in a rail [18]. In this case the orthogonality of mode shapes computed by SAFE analysis is used. If the time response at all degrees of freedom at a cross – section of the

waveguide could be measured the time signal for a selected mode could be obtained by summing all the response signals with a weight function that is the mode shape of the selected mode. Typically it is only possible to measure the responses at a small fraction of the degrees of freedom so perfect single mode detection is not possible although additional measurements at different distances could be included. Unfortunately, results from the application of this method to rails have not been found in the literature. Unlike the case of a cylinder, the mode shapes of a rail are not constant with frequency. However, the mode shapes can be computed, as functions of frequency, by numerical methods such as the SAFE method, which also provides the wavenumber – frequency relations for the modes. If we have an accurate model we can use this information to extract (or estimate) the amplitudes of the modes contributing to experimentally measured signals in the frequency domain. This approach is believed to be appropriate for the application of measuring attenuation of individual modes with distance and for evaluating the performance of transducers on waveguides that can be accurately modelled.

The use of a model to process independently measured signals is commonly performed in array processing [19]. We use this approach in this paper as the intention is to interpret our measurements in quantities that are described by the numerical models. A method is described for processing scanning laser vibrometer measurements, which may be thought of as a receive array, based on dispersion characteristics obtained from SAFE model computations. Particular aspects required for accurate measurements are discussed and example results are presented.

The mode measurement method is presented in section 2 while laboratory and field measurement results are described in section 3. Section 4 contains some findings and tips for performing the measurements in practice and for applying the mode measurement technique, while conclusions are presented in section 5.

2. MODE EXTRACTION THEORY

The mode estimation technique requires accurate information about the propagating waves. Analytical solutions for the propagating modes of simple geometries are available but a complex geometry, such as a rail, requires numerical analysis. The SAFE method has become very popular for this type of analysis. In this method, the finite elements are formulated including a complex exponential function to describe the variation of the displacement field along the waveguide and conventional finite element interpolation functions are used over the area of the element. This means that only a two-dimensional finite element mesh of the waveguide cross-section is required. The displacement fields (u_x, u_y, u_z) in an elastic waveguide, extending in the z direction, can be written as;

$$\begin{aligned} u_x(x,y,z,t) &= u_x(x,y)\cdot e^{-j(\kappa z-\omega t)} \\ u_y(x,y,z,t) &= u_y(x,y)\cdot e^{-j(\kappa z-\omega t)} \\ u_z(x,y,z,t) &= j\cdot u_z(x,y)\cdot e^{-j(\kappa z-\omega t)} \end{aligned} \tag{1}$$

where, z is the coordinate in the direction along the waveguide, κ the wavenumber and ω the angular frequency. Application of conventional finite element interpolation functions over the cross-section results in the system of equations of motion $M\ddot{u}+\left[\kappa^2\cdot K_2+\kappa\cdot K_1+K_0\right]u=0$. The displacement vector u contains nodal displacements in the x, y and z directions. The mass matrix (M) is derived from the kinetic energy and the stiffness matrix, which is dependent on the wavenumber (κ), is derived from the strain energy. The stiffness matrix is separated into three stiffness matrices where K_2 is multiplied by the square of the wavenumber, K_1 is multiplied by

the wavenumber and K_0 is not multiplied by the wavenumber. The particular choice of functions in equation 1 was selected by Gavrić [2] to produce symmetric matrices. If the imaginary number j is omitted from the third equation in equation 1 the matrix K_1 will be skew-symmetric but can be transformed to be symmetric [3]. If harmonic motion is assumed and the equations of motion are complemented with an identity then equation 2 results and the solution at a particular frequency may be obtained.

$$\begin{bmatrix} K_0 - \omega^2 M & 0 \\ 0 & -K_2 \end{bmatrix} \begin{Bmatrix} u \\ \kappa u \end{Bmatrix} + \kappa \begin{bmatrix} K_1 & K_2 \\ K_2 & 0 \end{bmatrix} \begin{Bmatrix} u \\ \kappa u \end{Bmatrix} = \begin{Bmatrix} 0 \\ 0 \end{Bmatrix} \tag{2}$$

The eigenvalue problem in equation 2 may be solved, at a specified angular frequency (ω), to provide the mode shapes (ψ_l) and corresponding wavenumbers (κ_l). Real values of wavenumber indicate propagating modes and these are the modes used in the mode estimation process. Since imaginary and complex wavenumbers, which correspond to modes with exponential decay over distance, are not used the process is only applicable to measurement regions away from irregularities.

The frequency response of the waveguide at degree of freedom *i*, away from irregularities and the excitation source, can be written as a superposition of the *m* forward propagating modes and *m* backward propagating modes:

$$r_i(z,\omega) = \sum_{l=1}^{2m} \psi_{il}(\omega) e^{-j\kappa_l(\omega)z} \alpha_l(\omega) \tag{3}$$

where $\psi_{il}(\omega)$ is the displacement of degree of freedom *i* of mode shape *l* and $\kappa_l(\omega)$ is the wavenumber of mode *l*. The complex quantity $\alpha_l(\omega)$ is the modal coefficient for mode *l* and represents the magnitude and phase of that mode as a function of frequency. A SAFE analysis of the rail provides the terms $\psi_{il}(\omega)e^{-j\kappa_l(\omega)z}$. Both forward and backward propagating modes are superimposed in order to take account

of reflections from irregularities, such as distant welds, which may be present in the measured signals.

Measurements may be performed at a single frequency using a continuous sine wave excitation or by using a short time signal that contains a range of frequencies. We wish to estimate the magnitude and phase of each propagating mode ($\alpha_l(\omega)$) from experimental time response measurements. If we perform measurements at *p* different points, each at a known distance (*z*) and location on the rail surface and in a particular displacement direction, the response can be written as a superposition of the contributions of the forward and backward propagating modes, which can be written in the form $D(\omega)\alpha(\omega) = r(\omega)$ as shown in equation 4. In equation 4, the subscripts *f* and *b* are used to indicate forward and backward propagating modes respectively.

$$\begin{bmatrix} \psi_{11f}(\omega)e^{-j\kappa_{1f}(\omega)z_1} & \cdots & \psi_{1mf}(\omega)e^{-j\kappa_{mf}(\omega)z_1} & \psi_{11b}(\omega)e^{-j\kappa_{1b}(\omega)z_1} & \cdots & \psi_{1mb}(\omega)e^{-j\kappa_{mb}(\omega)z_1} \\ \vdots & \vdots & \vdots & \vdots & \vdots & \vdots \\ \psi_{p1f}(\omega)e^{-j\kappa_{1f}(\omega)z_p} & \cdots & \psi_{pmf}(\omega)e^{-j\kappa_{mf}(\omega)z_p} & \psi_{p1b}(\omega)e^{-j\kappa_{1b}(\omega)z_p} & \cdots & \psi_{pmb}(\omega)e^{-j\kappa_{mb}(\omega)z_p} \end{bmatrix} \begin{Bmatrix} \alpha_{1f}(\omega) \\ \vdots \\ \alpha_{mf}(\omega) \\ \alpha_{1b}(\omega) \\ \vdots \\ \alpha_{mb}(\omega) \end{Bmatrix} = \begin{Bmatrix} r_1(\omega) \\ \vdots \\ r_p(\omega) \end{Bmatrix} \quad (4)$$

The mode shape matrix *D* is assembled from information obtained from the SAFE model while the response vector *r* is assembled by performing a FFT on each of the measured time domain signals. Note that the mode shape matrix, the modal coefficients and the frequency responses are all complex quantities. If velocities are measured instead of displacements these can be simply converted to displacements by dividing by $j\omega$. Matrix *D* has dimension [*p* x *2m*], while α is [*2m* x 1] and *r* is [*p* x 1]. If *p* is equal to *2m* (number of measurement points equal to number of modes) the matrix *D* is square and can be inverted. However, we expect a better result if we use additional measurement points (*p* > *2m*). This produces more equations than we have unknowns and the non – square matrix *D* cannot be simply inverted. All the

equations cannot be satisfied exactly and we can only solve the over-defined system of equations in a least-squares sense. This can be conveniently achieved by using the Moore-Penrose generalized inverse (also called the pseudo inverse). We expect that the matrix *D* will be rank *2m* if there are at least *2m* different propagating modes at the frequency of interest. The generalized inverse of *D*, in this case, is $D^{\dagger} = [D^{*}D]^{-1}D^{*}$, where *D** is the Hermitian transpose of *D* and an estimate of α is obtained from equation 5.

$$\tilde{\alpha} = D^{\dagger} r \,. \tag{5}$$

The quality of the fit of the model data to the experimental data can be checked by computing the displacements at each scan point from the mode shape matrix and the estimated modal coefficients.

$$D(\omega)\tilde{\alpha}(\omega) = \tilde{r}(\omega) \tag{6}$$

In this way we can measure how well the extracted values fit the measured values and we can define an average mean squared error:

$$ERROR(\omega) = \frac{1}{p}\left[\{r(\omega) - \tilde{r}(\omega)\}^{*} \cdot \{r(\omega) - \tilde{r}(\omega)\}\right]^{\frac{1}{2}} \tag{7}$$

Equation 7 is useful if we are interested in only one frequency as is the case when we perform field measurements with continuous sinusoidal excitation. If we excite with a short time signal and wish to determine how well the estimated data agrees with the measured time signals we can transform the estimated frequency responses back to the time domain using the inverse Fourier transform as shown in equation 8. The estimated time responses can then be plotted with the measured time responses and this is done for the lab measurements in section 3.2.

$$\tilde{r}(t) = IFFT(\tilde{r}(\omega)) \tag{8}$$

3. EXAMPLE RESULTS

For long range guided wave propagation in rail track we are typically interested in the frequency range between 30 kHz and 40 kHz. Measurements were performed on a 5m long rail (UIC60 profile) in the laboratory and on an operational rail track (with S-60-SAR profile) and example results are presented in this section. The measurements were performed using a Polytec PSV-400-M2-20 high frequency scanning vibrometer equipped with the VD-09 velocity decoder having a typical resolution of 0.7 μm/s/√Hz. In addition, the system was equipped with a geometry scan unit that may be used to measure the physical positions of the scan points.

3.1 Lab Measurements

A custom developed piezoelectric sandwich transducer comprising a back mass, four piezoelectric ceramic rings, a front mass and a centre bolt was used to excite the rail. The transducer, which resembles an ultrasonic cleaning transducer, was attached under the head of the rail to provide an excitation in the vertical direction. This excitation is suitable for exciting modes that have significant motion in the head in the vertical direction but will not excite horizontal modes or modes that are predominantly in the foot of the rail. Two 17.5 cycle tone burst signals with centre frequencies of 25 kHz and 35 kHz respectively were used. A scan was performed to measure the vertical velocity at 223 measurement points located in the 0.83 m long scan region illustrated in figure 1, which includes a section of the head of the rail and a section on the foot to each side of the head. The measurement points were distributed in two lines along each foot and three lines along the head with an axial spacing of between 0.025 m and 0.03 m. The velocities were used to estimate the forward and backward propagating modes using equation 5. Additional measurements

were performed outside of the scan region at points designated C1 and C2 in figure 1. These points were not used in the mode measurement process but were used to provide a check of the accuracy of the estimated modal coefficients by using these coefficients to reconstruct or predict the displacements at these points.

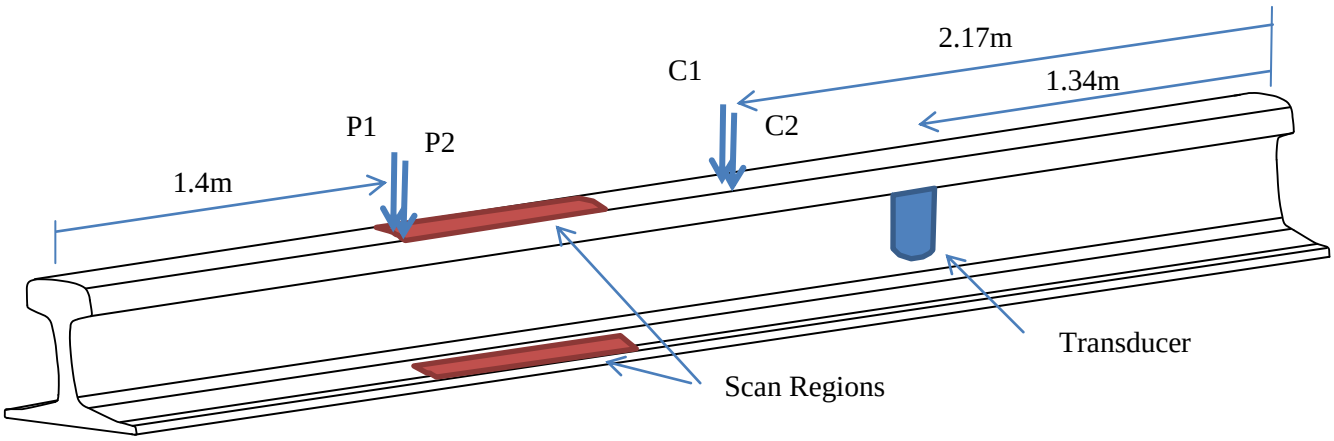

Figure 1. Experimental setup on 5m long rail in the lab.

Figure 2 shows the displacement signals obtained from the measured velocities at two measurement points P1 and P2 at the left edge of the scan region. Points P1 and C1 are near the axis of symmetry while P2 and C2 are away from the axis of symmetry. A SAFE model with an elastic modulus of 205 GPa was used to compute the mode shape matrix. The estimated modal coefficients were used to reconstruct the displacements at these points using equation 6 and these signals are included in figure 2. Note that only propagating modes with real wavenumbers were used in this process so attenuation due to material absorption is not included while dispersion is included. In these figures the time signals are the real part of $\tilde{r}(t)$ computed using equation 8 while the wave packet envelope is obtained by plotting the absolute of $\tilde{r}(t)$.

The modal coefficients were used to predict the displacements at C1 and C2 and are compared to actual measurements at these locations in figure 3. It is observed that the

extrapolation on the axis of symmetry is very good while that off axis resembles the measurement but the agreement is worse. This is to be expected as the vertical response on the axis of symmetry is due to the symmetric modes only while the response off axis is a combination of the symmetric and the anti-symmetric modes. Most of the energy in the 25 kHz centre frequency signal is contained between 22.5 kHz and 28 kHz and only this frequency range was used. At 22.5 kHz there are 16 propagating modes in each direction, while at 28 kHz there are 20 propagating modes in each direction. The estimated responses are a linear combination of the response of each mode and it is possible to determine the contribution of each mode separately. This feature is illustrated in figure 4 were only the wave packet envelopes are plotted for clarity. It was found that at 25 kHz centre frequency the response on the axis of symmetry is dominated by a single mode of propagation. The response of this mode in the forward and backward directions and the combined response are plotted in figure 4a. In this response we observe that the backward propagating mode arrives first at 1.2 ms, then again at 2.1 ms (reflection from right end) and again at 4.5 ms (reflection off left end then off right end). The time difference between the first and third arrival is 3.3 ms which corresponds to a distance of 10 m (twice the length of the rail) for this mode, which has a group velocity of 3041 m/s at 25 kHz. This 3.3 ms interval is observed in other peaks too. In the case of the off-axis measurement point it was found that most of the response can be attributed to the symmetric mode and two of the anti-symmetric modes. The combined response of these three modes in the forward and backward direction is illustrated in figure 4b.

1

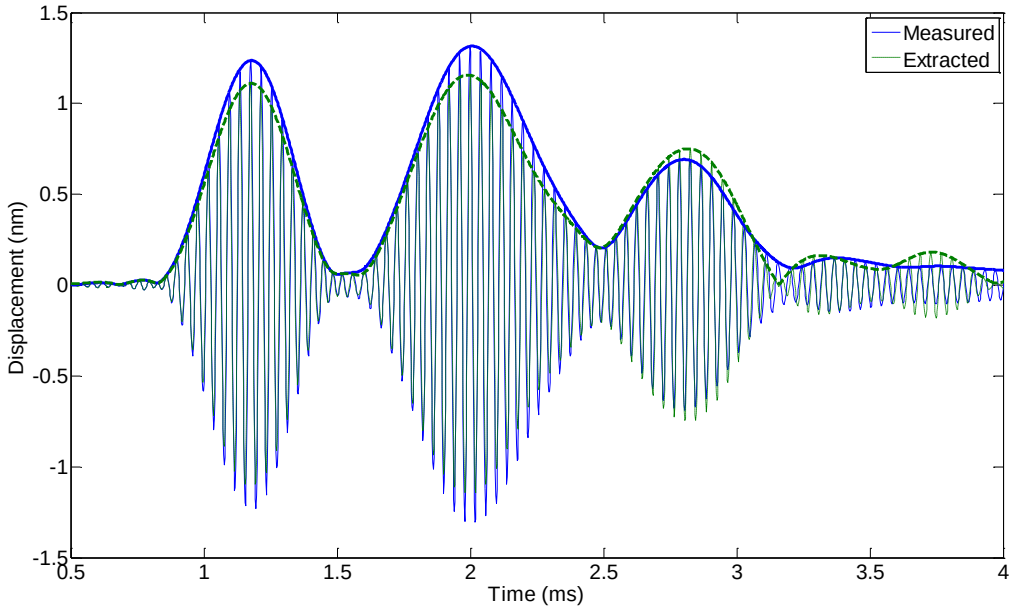

2
3 a)

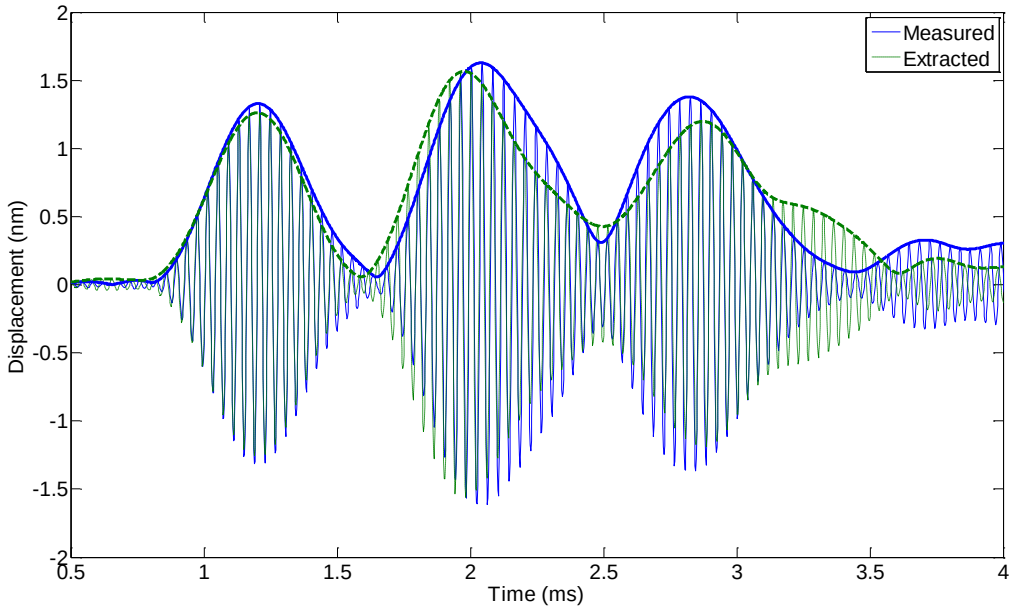

4
5 b)

6 **Figure 2.** 25 kHz Measurement and Estimated Result a) P1 near axis, b) P2 off axis.

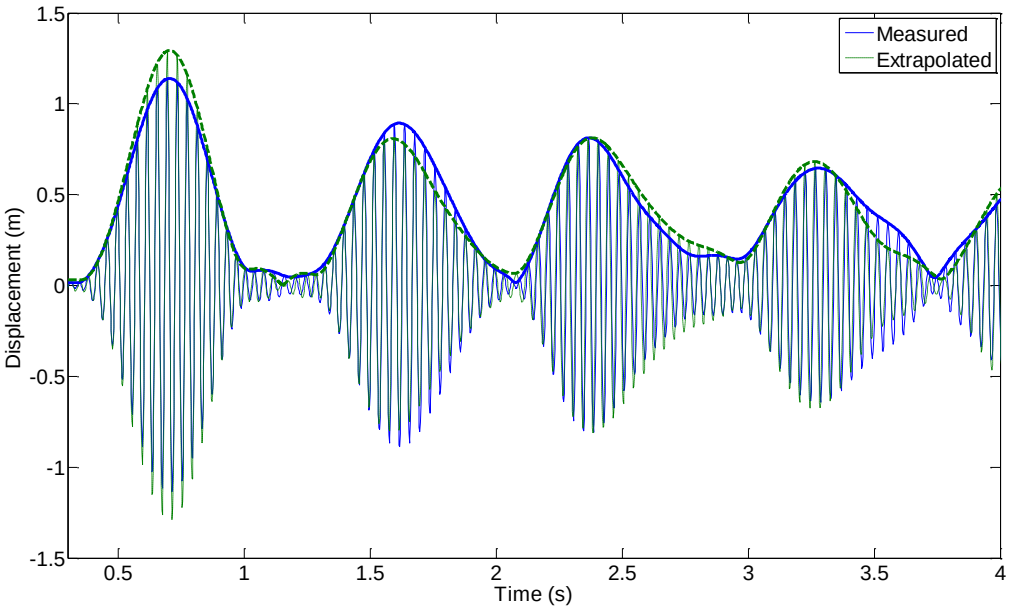

a)

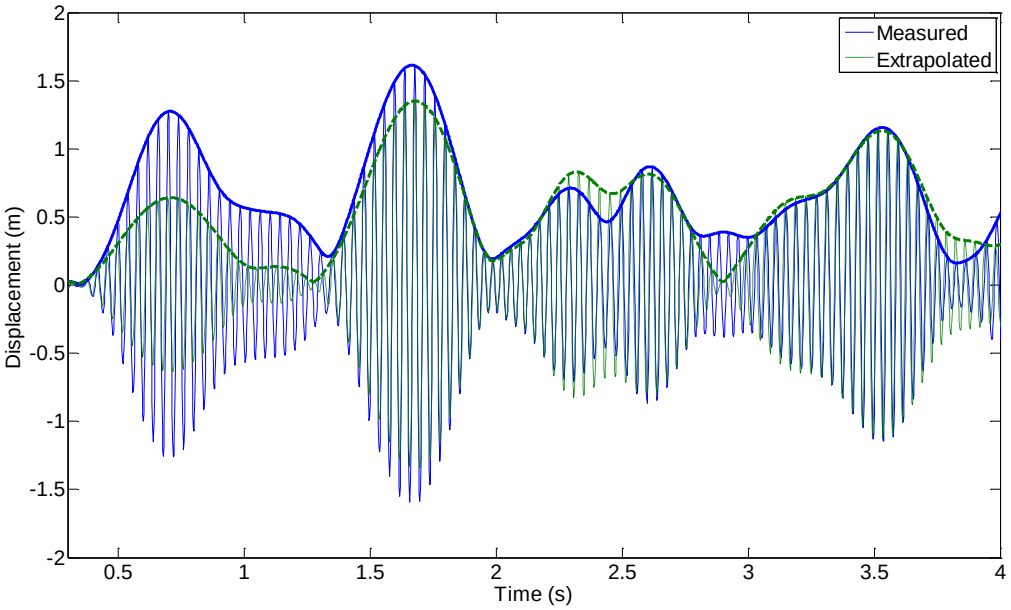

b)

Figure 3. 25 kHz Measurement and Extrapolated Result a) C1 near axis, b) C2 off axis.

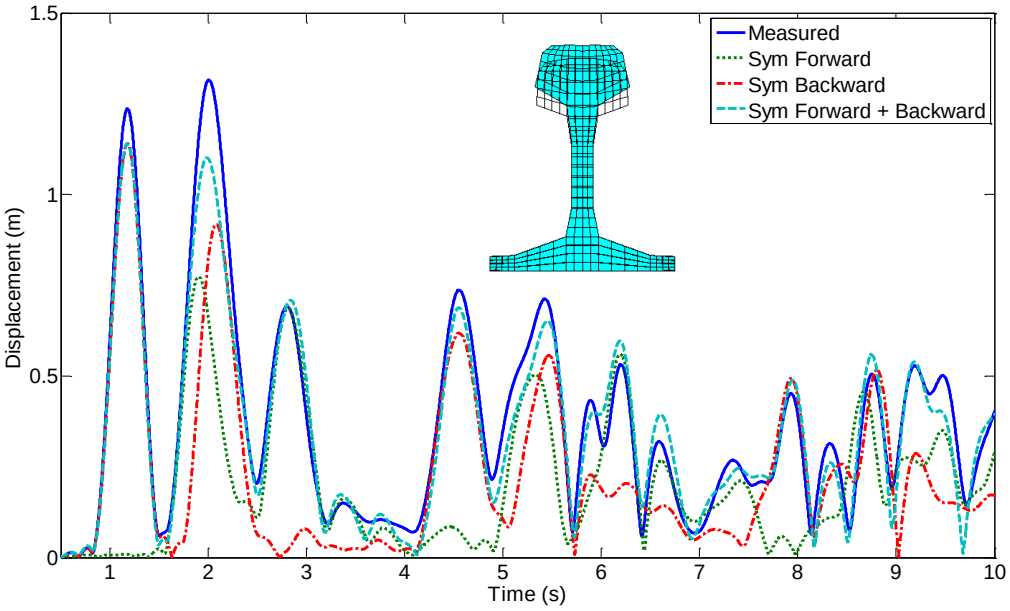

a)

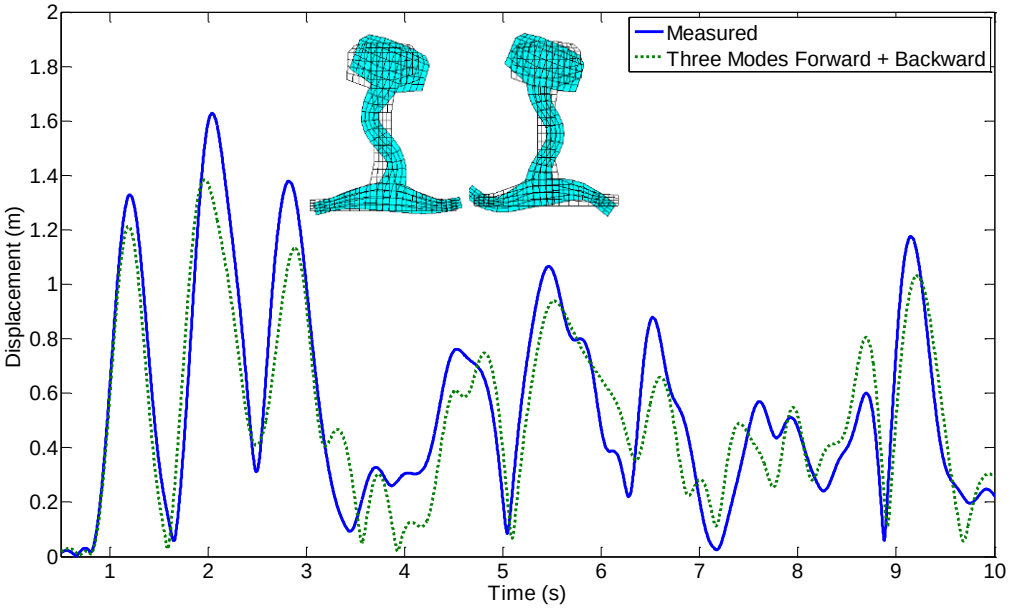

b)

Figure 4. 25 kHz Measurement and Estimated Result a) P1 near axis, one mode contribution, b) P2 off axis, three mode contribution

The process was repeated with the 35 kHz centre frequency signal and the measured and reconstructed signals at points P1 & P2 are shown in figure 5. The measured and

extrapolated signals at the check points, C1 and C2, are shown in figure 6. It was observed that the situation is more complex at the higher frequency as there are more modes in the frequency range (20 modes increasing to 27 modes) and more modes contribute to the response. When a single mode of propagation is incident at a free end the reflection can contain numerous modes propagating in the opposite direction and not only the incident mode. This mode coupling at a free end has been predicted to be significantly more pronounced at 35 kHz than at 25 kHz, using the modelling method applied at lower frequencies in [20], which adds to the complexity of the wave propagation.

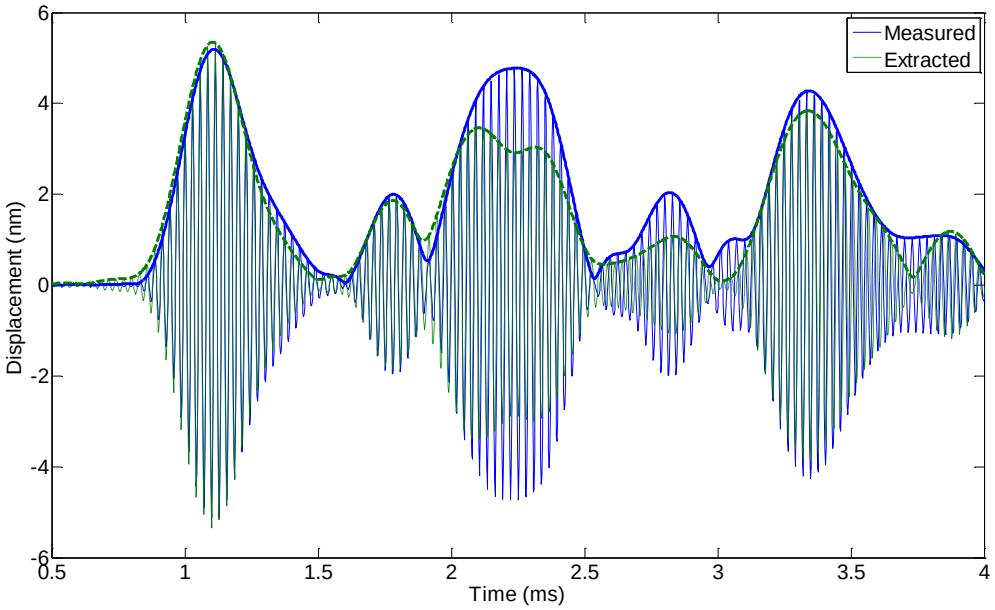

a)

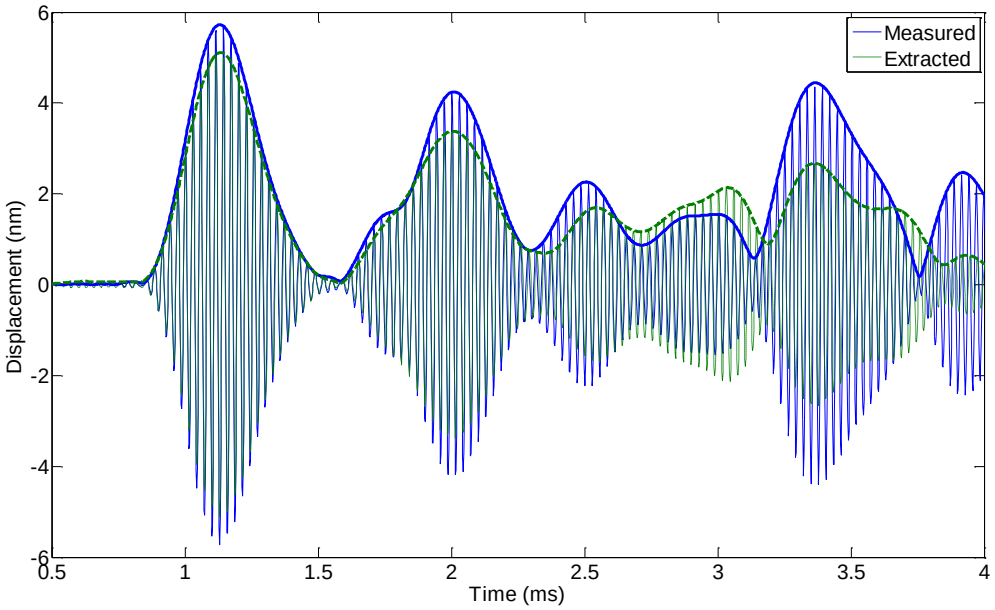

b)

Figure 5. 35 kHz Measurement and Estimated Result a) P1 near axis, b) P2 off axis.

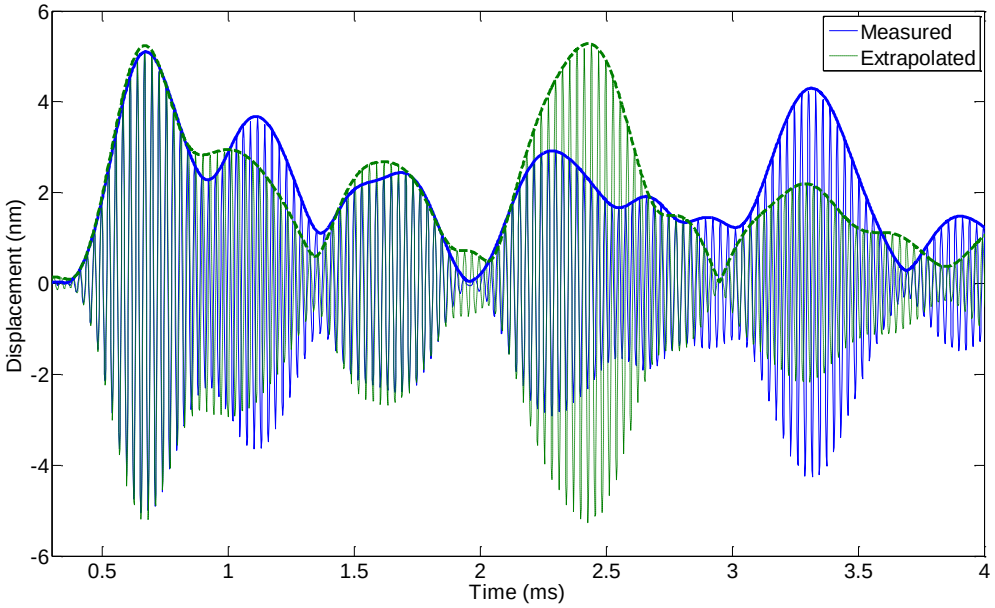

a)

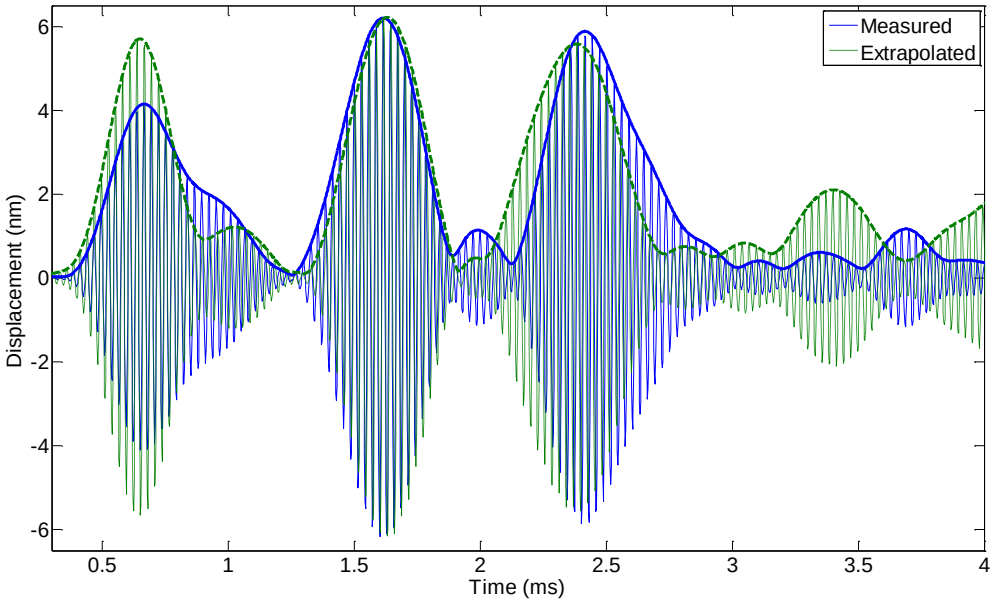

b)

Figure 6. 35 kHz Measurement and Extrapolated Result a) C1 near axis, b) C2 off axis

3.2 Field Measurements

Measurements were performed on an operational continuously welded rail line with the purpose of evaluating the attenuation of particular modes with distance. This was achieved by performing scans at different distances from a transmit transducer. The transmit transducer was attached under the crown of the rail to excite in the vertical direction similar to the lab experiment. The rail was in poor condition having been repaired on numerous occasions. The repairs involve welding a replacement length of at least 6m with two alumo – thermite welds. These welds have since been shown to reflect guided waves even when they are performed in new rail. When a new section of rail is welded into old rail with significant profile grinding the step change in profile causes an even greater reflection [21]. The measurements were performed using a continuous excitation of the transducer at a single frequency to obtain a high signal to noise ratio and to avoid dispersion. Distances of up to 500m between the transmit transducer and the scan region were used. As there was no connection between the transmit station and the receive station a reference transducer was attached to the rail near the scan region to provide a phase reference for the laser vibrometer.

A scan performed at a distance of 400m from a transducer excited at 30 kHz is shown in figure 7. This scan included 405 measurement points on the foot and crown of the rail. It should be noted that the peak velocity measured was approximately 35 μm/s, which corresponds to a peak displacement of approximately 0.2 nm at 30 kHz. The frequency resolution used was 31.25 Hz and four measurements were averaged to improve the signal to noise ratio.

The modes were estimated at 30 kHz and the amplitudes of the forward and backward propagating modes are listed in table 1. The mode shape vectors were scaled to have unity maximum therefore the tabulated amplitudes are the maximum displacement amplitude for each propagating mode. Modes 3 and 11 had no motion in the vertical direction at the measurement points and were excluded from the estimation process. It was found that two modes (4 & 7), one symmetric and one anti-symmetric, propagate large distances even in old rail containing numerous welded repairs. Scattering at the welds is believed to be responsible for greater attenuation of these modes (up to 80 dB/km) than would be expected from material absorption alone where a minimum attenuation of 40 dB/km has been predicted for one of these modes [7]. The SAFE method predicted dispersion curves computed for this rail and the two modes are shown in figure 8. The symmetric mode in figure 8 is similar to the symmetric mode measured in the lab but has more bending deformation across the width of the head which is thinner due to rail profile grinding performed on the rail in the field. The transducers used in both experiments were designed and positioned to excite this symmetric mode so it is not surprising that this mode is present in the response. The anti-symmetric mode shown in figure 8 is similar to the first anti-symmetric mode shown in figure 2b but has less motion in the foot of the rail. This mode is therefore likely to have low attenuation at this frequency in rail where significant profile grinding has been performed but would have greater attenuation in new rail.

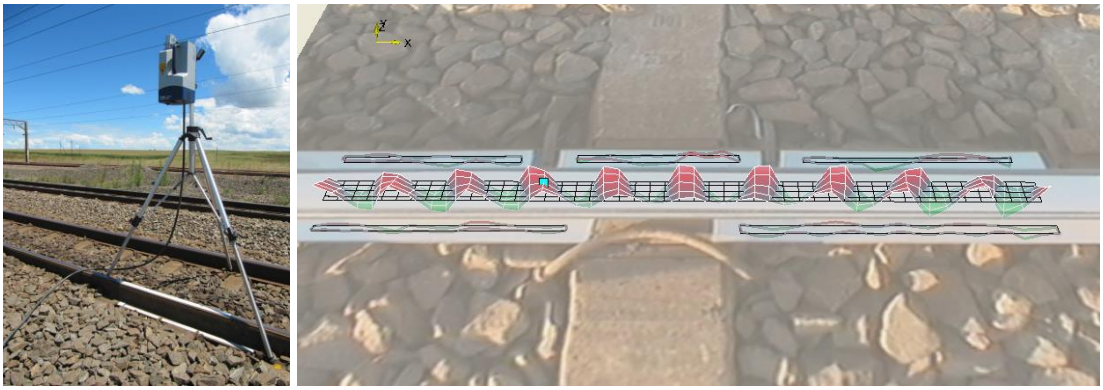

Figure 7. Scanning head positioned above rail and scan result at 30 kHz and 400m from excitation transducer.

TABLE 1. Extracted mode amplitudes 30 kHz

Mode No.	Wavenumber (rad/m)	Forward Amplitude (Mode 3 & 11 excluded) (nm)	Backward Amplitude (Mode 3 & 11 excluded) (nm)
1	99.22	0.45	0.10
2	99.19	0.35	0.01
3	90.67	-	-
4	**78.03**	**3.16**	**0.07**
5	73.84	0.21	0.04
6	74.43	2.03	0.17
7	**72.25**	**5.61**	**0.34**
8	69.22	0.45	0.01
9	64.12	0.44	0.23
10	54.90	0.20	0.07
11	54.77	-	-
12	48.92	0.04	0.02
13	40.52	0.37	0.11
14	37.25	1.42	0.19
15	36.04	0.34	0.11
16	32.99	0.88	0.12
17	25.37	0.42	0.08
18	24.41	0.57	0.07
19	17.13	0.36	0.22

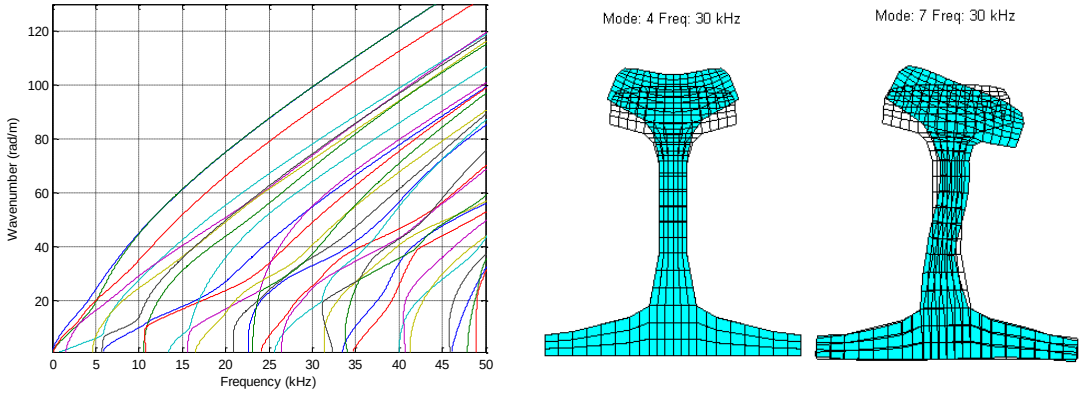

Figure 8. Dispersion curves computed for measured rail and mode shapes of modes that propagate large distances.

The fit of the response reconstructed from the estimated modal coordinates to the measured data is illustrated in figure 9. The real and imaginary components of the measured response at the scan points are shown (figure 9a & b) and the estimated response reconstructed from the estimated modal coordinates is shown (figure 9c & d) again as real and imaginary components. It is observed that the estimated response on the crown agrees very well with the measured response. The response at points on the foot of the rail is significantly smaller than the response on the crown and some differences between the estimated response and the measured response can be identified.

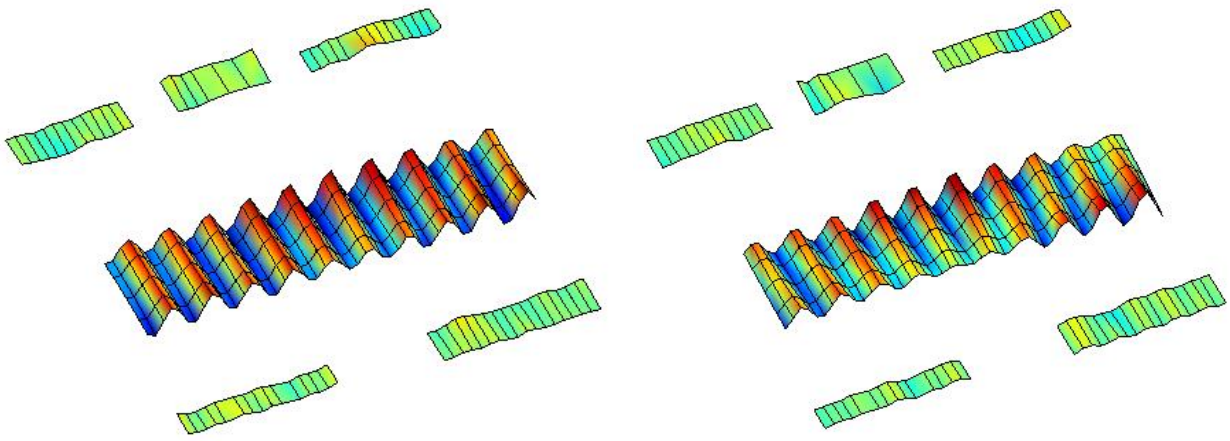

a) b)

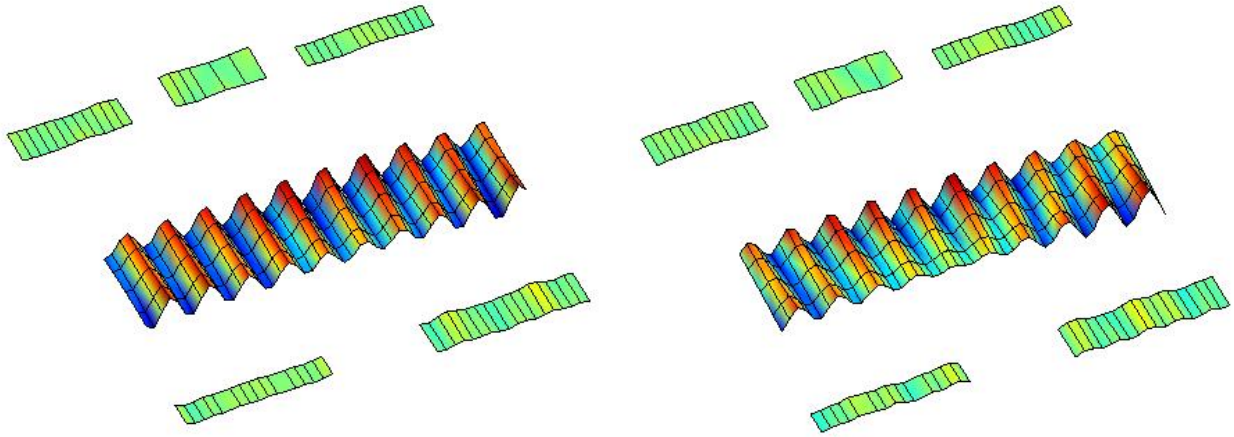

c) d)

Figure 9. Measured and estimated field measurement responses, a) measured real component, b) measured imaginary component, c) estimated real component and d) estimated imaginary component.

4. IMPLEMENTATION LESSONS

Measurement of small displacements in the field at large distances from the excitation transducer was achieved by using a continuous sine wave excitation at a single frequency and measuring the response at this frequency. In this way noise at all other frequencies is eliminated. It was easier to measure velocities and then convert these to displacements at that particular frequency than to measure displacements directly in the field, as there can be large low frequency motions that can cause signal saturation. Averaging was used but only between 4 and 8 averages were used in the field as this increases the time required for a scan. The time for a scan was typically between 10 and 20 minutes with the shorter time scans being less likely to be interrupted by a passing train.

The displacements at the scan points are measured sequentially and a phase reference is required to obtain the relative phase at each measurement point. Usually the excitation signal applied to excite the ultrasonic transducer would be used as a phase

reference, but this was not available as the transmit station was up to 500m away from the scan region. Instead, a second transducer was attached near the scan region and this signal was used as the phase reference.

A good retroreflective surface is required on the scan region which was approximately 1m long. Reflective fabric used in the manufacture of high visibility safety clothing was used and adhered to the rail with 90 micron thick double sided tape. The reflective tape on the rail crown had to be replaced after each passing train so a considerable amount was used. Using the reflective fabric and double sided tape was significantly cheaper than using the A4 sized reflective sheets supplied by laser vibrometer manufacturer.

Initially, an attempt was made to perform scanning laser vibrometer measurements at points, on the rail surface, that coincide with nodal locations in the SAFE model. However, it proved to be difficult to align the scanning head with the rail and to control the position of the measurement points using the standard software available on the scanning laser vibrometer system. Instead, the scan grid was specified using the system software and then the location of selected points on the rail surface was measured and used to interpolate the positions of the rest of the scan points. As the measurement locations did not coincide with nodes in the SAFE model, the SAFE mode shape vectors were interpolated to coincide with these measurement locations. In order to improve the accuracy of the scan point locations, a geometry scan unit was purchased and integrated with the scanning laser vibrometer system. This unit was used for the lab measurements presented here but an accuracy of only approximately 4 mm was achieved over the scan region. It would be beneficial if this could be

improved in future as the position of the scan points, especially the distance from the axis of symmetry of the rail, is very important for accurate estimation of the modal coordinates and also for achieving a low error as defined in equation 7. The scan region was typically about 0.8 m long and this is limited by the scanning mirror angles in the system and the distance between the scanning head and the rail. Longer scan regions would be beneficial if this can be achieved while keeping the laser relatively normal to the rail. Hayashi et al. [22] used a robotic arm to position a laser vibrometer sensor for measuring guided waves in a rail instead of using mirrors to scan the laser beam. This produced excellent position accuracy and also maintains the normal angle between the laser beam and the measurement surface.

We were primarily interested in modes of propagation that are mainly in the head of the rail and that travel long distances. The excitation used was appropriate for these modes. If modes in the foot or web of the rail are to be measured the excitation would have to be designed to excite these modes. Measurement of the horizontal motion of the web of the rail would be required to measure a mode confined to this part of the rail. It was found that even though we are mainly interested in modes of the head of the rail it was necessary to include measurements of the foot of the rail in the process. If only measurements on the crown are performed unrealistically large modal amplitudes result even though a low error as defined by equation 7 may be obtained. The number of measurement points required was studied in [23] where it was shown that increasing the number of points does not necessarily result in an improved result. Selecting only a small number of measurement points may result in a poor condition number of the mode shape matrix and unrealistic estimates of the modal coordinates even though the error as defined in equation 7 is low.

It was found to be very important to model the actual geometry of the rail cross section where the scan is performed. The field measurements were performed on very old rail where profile grinding had removed 12 mm of material from the top surface of the rail. It was not possible to obtain a low error (as defined in equation 7) until the geometry of the SAFE model was corrected to represent the actual geometry. The error can be further decreased by varying the elastic modulus of the rail. This was performed both for the lab measurements and the field measurements. The influence of the correct elastic modulus on obtaining the correct wavelength for the model is demonstrated in figure 10 for the lab measurements performed with a centre frequency of 35 kHz. In figure 10a an elastic modulus of 215GPa was used and the estimation process was able to fit the measured signal well at the centre of the scan region but had a phase lag at the left edge of the scan region and a phase lead at the right edge of the scan region indicating that the model wavelength was incorrect. The elastic modulus was changed to 205GPa and the superior fit shown in figure 10b was obtained.

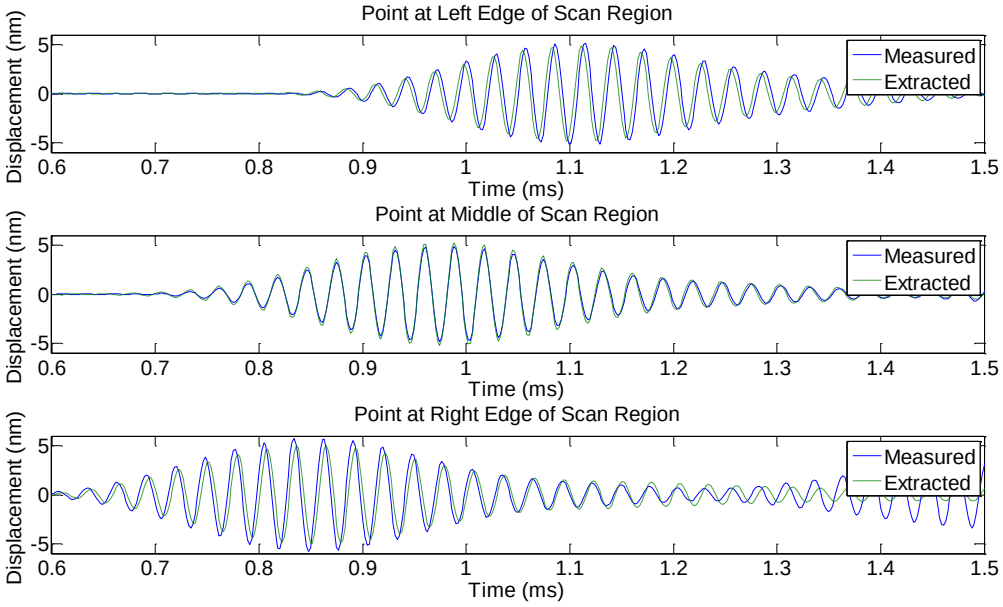

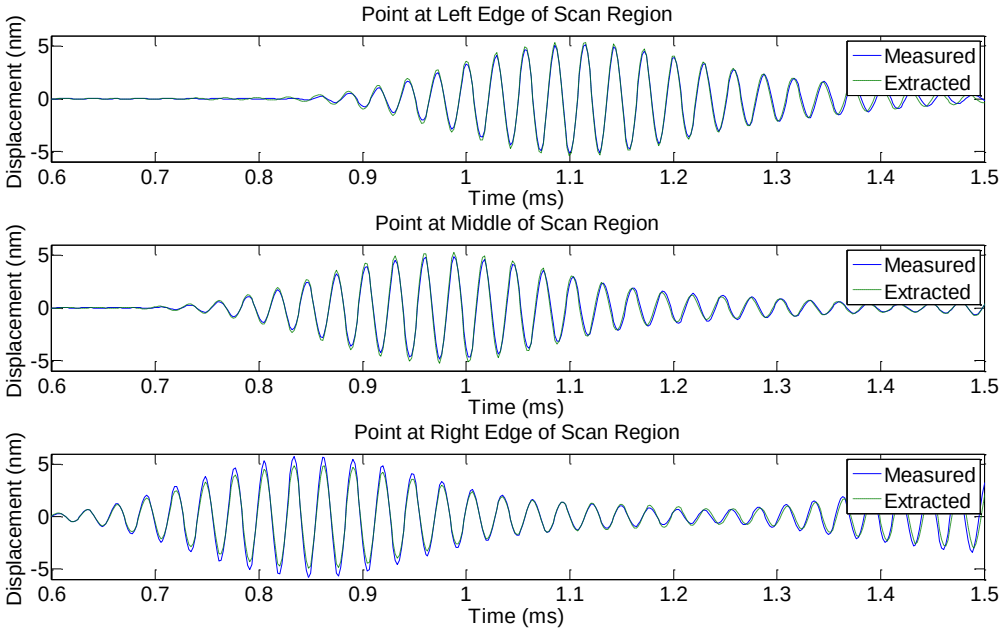

Figure 10. Measured and estimated signals for elastic modulus of a) 215 GPa and b) 205 GPa.

The quality of the fit to the field measurements was also improved by adjusting the elastic modulus. Figure 11 shows the error as a function of elastic modulus and the improvement in the fit at the measurement points was clearly visible [24]. It appears that the old rail measured in the field had a higher elastic modulus than the new rail used in the lab. These two rails had different profiles and were most probably produced by different manufacturers.

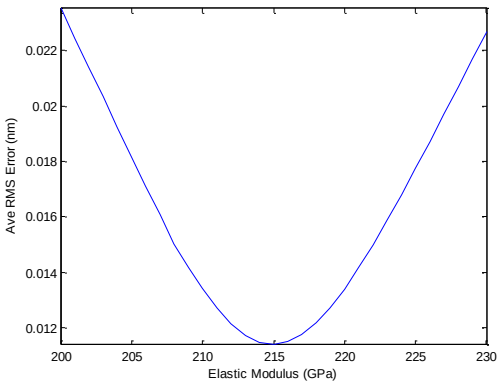

Figure 11. Influence of elastic modulus on error in fitting field measurement results.

5. CONCLUSIONS

A method to estimate the modal coordinates from time domain laser vibrometer measurements exploiting SAFE model information was investigated. The modes of propagation were measured, on a 5 m length of rail excited by custom transducers, in the lab using tone burst excitation with 25 kHz and 35 kHz centre frequency. The mode measurement was more effective at the lower frequency where the response is dominated by only a few modes of propagation. The estimated modal amplitudes were used to predict the response at additional locations along the rail and the agreement with measurements was satisfactory. It is believed that the method is sufficiently accurate for comparing the performance of different transducer designs in the lab.

Field experiments were performed and two modes that propagate large distances in rail track in poor condition were measured at a distance of 400m from the transducer. The small displacements at this distance had amplitude of the order of only 0.2 nm at 30 kHz but could be measured using a laser vibrometer.

It was found that a relatively accurate model of the propagating modes is required in order to obtain a low error between the estimated and measured responses. Large geometric changes such as those produced by profile grinding should be included in the model, after which the elastic modulus used in the model can be varied to further reduce the error. Updating the model parameters automatically could be investigated in future especially if it is suspected the properties vary over the cross-section, for example due to hardening of the running surface.

One of the difficulties experienced during application of the method is obtaining an accurate measure of the positions of the measurement points relative to the axis of symmetry of the rail. Accurate measurement of the scan locations is required to ensure that the correct displacement components from the SAFE analysis are used in the process.

Results presented here were mainly focussed on measuring modes that propagate with most of the energy concentrated to the rail head and which are excited in the vertical direction. Other modes such as one that propagates mainly in the web of the rail could be measured if horizontal displacements are measured and the excitation is adapted to excite this mode.

The method has provided useful information for designing monitoring systems by providing estimates of the attenuation of specific modes in the field and by characterising the performance of transducers in the lab.

ACKNOWLEDGEMENTS

Access to the railway track for field measurements was provided by Transnet Freight Rail and is gratefully acknowledged. Funding for this project was provided by the CSIR, the Department of Science and Technology and the National Research Foundation of South Africa (Grant No's: 78858 & 85330).

REFERENCES

[1] P. W. Loveday, Guided Wave Inspection and Monitoring of Railway Track, J. Nondestruct. Eval. 31(4) (2012) 303–309.

[2] L. Gavric, Computation of propagative waves in free rail using a finite element technique, J. Sound Vib. 185(3) (1995) 531–543.

[3] V. Damljanović and R. L. Weaver, Propagating and evanescent elastic waves in cylindrical waveguides of arbitrary cross section, J. Acoust. Soc. Am. 115(4) (2004) 1572-1581.

[4] T. Hayashi, W.-J. Song, and J. L. Rose, Guided wave dispersion curves for a bar with an arbitrary cross-section, a rod and rail example, Ultrasonics 41(3) (2003) 175–183.

[5] I. Bartoli, A. Marzani, F. Lanza di Scalea, and E. Viola, Modeling wave propagation in damped waveguides of arbitrary cross-section, J. Sound Vib. 295 (2006) 685–707.

[6] P. W. Loveday, Semi-analytical finite element analysis of elastic waveguides subjected to axial loads, Ultrasonics 49(3) (2009) 298–300.

[7] J. Ryue, D. J. Thompson, P. R. White, and D. R. Thompson, Decay rates of propagating waves in railway tracks at high frequencies, J. Sound Vib. 320 (2009) 955–976.

[8] M. Mazzotti, A. Marzani, I. Bartoli, and E. Viola, Guided Waves dispersion analysis for prestressed viscoelastic waveguides by means of the SAFE method, Int. J. Solids Struct. 49(18) (2012), 2359-2372.

[9] V. Baronian, A. Lhémery, and a.-S. Bonnet-BenDhia, Simulation of non-destructive inspections and acoustic emission measurements involving guided waves, J. Phys. Conf. Ser. 195, (2009).

[10] F. Benmeddour, F. Treyssède, and L. Laguerre, Numerical modeling of guided wave interaction with non-axisymmetric cracks in elastic cylinders, Int. J. Solids Struct. 48(5) (2011) 764–774.

[11] C. S. Long and P. W. Loveday, Analysis of guided wave scattering due to defects in rails using a hybrid FE-safe method, in Review of Progress in Quantitative Nondestructive Evaluation, 32 (2013) 238–245.

[12] P. W. Loveday, Analysis of piezoelectric ultrasonic transducers attached to waveguides using waveguide finite elements., IEEE Trans. Ultrason. Ferroelectr. Freq. Control, 54(10) (2007) 2045–2051.

[13] P. W. Loveday, Simulation of piezoelectric excitation of guided waves using waveguide finite elements, IEEE Trans. Ultrason. Ferroelectr. Freq. Control, 55(9) (2008) 2038–2045.

[14] D. N. Alleyne and P. Cawley, A two-dimensional Fourier transform method for the measurement of propagating multimode signals, J. Acoust. Soc. Am. 89(3) (1991) 1159–1168.

[15] D. Thompson, Experimental analysis of wave propagation in railway tracks, J. Sound Vib. 203(5) (1997) 867–888.

[16] F. Lanza di Scalea and J. McNamara, Measuring high-frequency wave propagation in railroad tracks by joint time–frequency analysis, J. Sound Vib. 273(3) (2004) 637–651.

[17] T. Hayashi and M. Murase, Mode extraction technique for guided waves in a pipe, Nondestruct. Test. Eval. 20(1) (2005) 63–75.

[18] T. Hayashi, C. Tamayama, and M. Murase, Wave structure analysis of guided waves in a bar with an arbitrary cross-section, Ultrasonics 44(1) (2006) 17–24.

[19] P. D. Wilcox, Guided-wave Array Methods, in Encyclopedia of Structural Health Monitoring, 2009.

[20] C. S. Long and P. W. Loveday, Numerical Characterisation of Guided Wave Scattering Due to Welds in Rails, in 18th World Conference on Nondestructive Testing (2012).

[21] P. W. Loveday and C. S. Long, Long range guided wave defect monitoring in rail track, in Review of Progress in Quantitative Nondestructive Evaluation 33 (2014) 179–185.

[22] T. Hayashi, Y. Miyazaki, M. Murase and T. Abe, Guided wave inspection for bottom edge of rails, in Review of Progress in Quantitative Nondestructive Evaluation, 26 (2007) 169–177.

[23] P. W. Loveday and C. S. Long, Modal amplitude extraction of guided waves in rails using scanning laser vibrometer measurements, in Review of Progress in Quantitative Nondestructive Evaluation 31 (2012) 182-189.

[24] P. Loveday and C. Long, Scanning laser vibrometer measurement of guided waves in rails, in 18th World Conference on Nondestructive Testing (2012).